HEALTH AND MEDICINE

Mass spectrometry imaging of the in situ drug release from nanocarriers

Jinjuan Xue[1,2], Huihui Liu[1], Suming Chen[1,3]*, Caiqiao Xiong[1]*, Lingpeng Zhan[1], Jie Sun[1], Zongxiu Nie[1,2]*

It is crucial but of a great challenge to study in vivo and in situ drug release of nanocarriers when developing a nanomaterial-based drug delivery platform. We developed a new label-free laser desorption/ionization mass spectrometry (MS) imaging strategy that enabled visualization and quantification of the in situ drug release in tissues by monitoring intrinsic MS signal intensity ratio of loaded drug over the nanocarriers. The proof of concept was demonstrated by investigating the doxorubicin (DOX)/polyethylene glycol–MoS₂ nanosheets drug delivery system in tumor mouse models. The results revealed a tissue-dependent release behavior of DOX during circulation with the highest dissociation in tumor and lowest dissociation in liver tissues. The drug-loaded MoS₂ nanocarriers are predominantly distributed in lung, spleen, and liver tissues, whereas the accumulation in the tumor was unexpectedly lower than in normal tissues. This new strategy could also be extended to other drug-carrier systems, such as carbon nanotubes and black phosphorus nanosheets, and opened a new path to evaluate the drug release of nanocarriers in the suborgan level.

INTRODUCTION

The rapid development of nanotechnologies has enabled nanoparticles to be increasingly applied to biomedicine (1), especially in the application as drug carriers (2). The nanoscale drug carriers have the potential to protect small molecular anticancer drugs from rapid clearance in the bloodstream (3, 4), overcome the physiological barriers (5), and accumulate specifically in the tumor areas (6). These advantages have attracted much attention to developing more efficient and versatile organic/inorganic or hybrid nanoparticles to assist cancer diagnosis and treatment (7). To develop an efficient drug carrier, the investigation of its biodistribution and drug release behavior in a living model biosystem is prerequisite. However, this investigation is challenging in part because of the lacking of desirable analytical techniques that enable simultaneous tracking of the nanocarriers and their payload drugs (8). The traditional techniques, such as positron emission tomography, magnetic resonance imaging, and fluorescent imaging, have various limitations, including limited spatial resolution, complicated labeling processes, or difficulty in simultaneously tracking the nanocarriers and drug release (9). Matrix-assisted laser desorption/ionization (MALDI) mass spectrometry imaging (MSI) is a powerful label-free tool to map biological molecules, such as lipids (10, 11), metabolites (12), proteins (13), and drugs (14), directly from biological tissues. Our previous work has demonstrated that many nanomaterials such as carbon nanomaterials have the capability to produce characteristic MS signals upon the laser ablation, which could act as markers for tracking their distribution in tissues by laser desorption/ionization MSI (LDI MSI) (15). Theoretically, this kind of nanomaterial that could adsorb and transfer ultraviolet (UV) laser energy may also serve as a matrix to assist the ionization of payload drugs during the

LDI process (16). The idea of taking advantage of the matrix function of nanoparticles has been successfully applied in the study of stability of monolayer surface modifications on nanoparticles (17). This concurrent ionization is promising to simultaneously detect and image the nanocarriers and loaded drugs by matrix-free LDI MSI.

Two-dimensional (2D) graphene-like transition-metal dichalcogenide nanomaterials are a new generation of ultrathin 2D nanomaterials (18). Molybdenum disulfide (MoS₂) nanosheets as a member of this new family have gained increasing attention and have been successfully applied in the drug delivery system, which combined photothermal and chemotherapy for cancer, because of its low toxicity, ultrahigh near-infrared absorbance, and drug loading capacity (19, 20). In addition, MoS₂-based nanocarriers also exhibited great potential in gene therapy and other combined therapies (21, 22). For example, the functionalized MoS₂ nanosheets could be used as a novel gene vector to load small interfering RNA (23) and DNA (24) for gene therapy. The designed MoS₂ composites combined with radiotherapy could completely destroy the tumors in mice (25). In addition, more and more inorganic nanocarriers, e.g., gold nanoparticles, carbon nanotubes, and the emerging black phosphorus nanosheets, have been developed and applied to biological systems, because of their high drug-loading efficiency and distinct advantages in combined therapy (26). Thus, the tracking of these nanocarriers and payload drugs in living systems is crucial for biomedical studies.

In the present study, we took the drug-loaded MoS₂ nanosheets as a proof of concept to show the possibility of LDI MSI approach to track both nanocarriers and drugs in tissues, thereafter to study in vivo and in situ drug release behavior. We discovered that LDI MSI could indeed simultaneously image the nanocarriers and their payload drugs in tissues based on the concurrently detected intrinsic characteristic MS peaks of MoS₂ nanosheets and payload anticancer drug doxorubicin (DOX), without using a label or tag. This strategy was also validated by the gold nanoparticles, carbon nanotubes, and black phosphorus nanosheets in nanocarrier-drug systems. The significance and features of this method are as follows: (i) first label-free approach for the simultaneous imaging of nanocarriers and

[1]Beijing National Laboratory for Molecular Sciences, Key Laboratory of Analytical Chemistry for Living Biosystems, Institute of Chemistry, Chinese Academy of Sciences, Beijing 100190, China. [2]University of Chinese Academy of Sciences, Beijing 100049, China. [3]Department of Neurology, Johns Hopkins University School of Medicine, Baltimore, MD 21224, USA.
*Corresponding author. Email: schen145@jhmi.edu (S.C.); xiongcq@iccas.ac.cn (C.X.); znie@iccas.ac.cn (Z.N.)

drug release in the suborgan level, (ii) in situ drug release in the tissues could be quantitatively evaluated by monitoring the change of intensity ratio of drug over nanocarriers, and (iii) this intensity ratio was observed directly proportional to the drug/carrier ratio, which allows the readout of drug release percentage with high resolution. By using this method, the quantitative investigation of the in situ drug release of the DOX/PEGylated MoS2 [polyethylene glyco (PEG)–MoS₂] experiment was carried out; the results revealed the different inter- and intratissue preferences of DOX/PEG-MoS₂ in normal and tumor-bearing tissues. The ion intensities of MoS₂ species can also be correlated directly to the amount of MoS₂ nanosheets present in tissues, which allowed for the quantification of the nanocarrier uptakes in organs and tumors.

RESULTS AND DISCUSSION
Characterization of MoS₂ nanosheets before and after drug loading
The MoS₂ nanosheets were synthesized by chemical exfoliation and sonication according to a previous report (27) and then PEGylated with lipoic acid–modified PEG (LA-PEG) to improve the stability and solubility of MoS₂ nanosheets in physiological conditions (19) (see the detailed synthetic process in the Supplementary Materials). Transmission electron microscopy (TEM) characterization showed the lateral size of synthetic MoS₂ nanosheets, and PEG-MoS₂ nanosheets (PEGylated nanosheets) were 750 ± 230 nm and 180 ± 45 nm, respectively (fig. S1). Then, the LDI behavior of these nanosheets

were investigated by LDI MS. Figure 1A shows the clear isotope pattern of Mo in negative ion mode upon laser ablation in a MALDI–time-of-flight (TOF) mass spectrometer. The further assignment with high-resolution (HR) MS suggested that these peaks belong to the oxide ions of MoS₂, e.g., $[MoS_2O]^-$ and $[MoS_2O_2]^-$, around the mass/charge ratios (m/z) of 177.8 and 193.8. Given that the slight oxidation of MoS₂ is very common in this nanomaterial (28), these characteristic oxide-negative ions could be used as specific markers to track the presence of MoS₂ nanosheets. Likewise, the PEGylated MoS₂ (PEG-MoS₂) nanosheets exhibited a similar MS pattern with bare MoS₂ nanosheets (Fig. 1B), which indicates that the PEG modification will not change the intrinsic structure of MoS₂ and that these PEG-MoS₂ nanosheets could also be detected by LDI MS.

DOX, as one of the common chemotherapy drugs, was loaded on the ultrathin large 2D surface of the PEG-MoS₂ nanosheets via hydrophobic interactions and π-π stacking (see the detailed loading procedure in the Supplementary Materials) (19). The successful drug loading can be seen from the characteristic adsorption peak at 490 nm belonging to DOX in UV-visible (vis) adsorption spectra of PEG-MoS₂ nanosheets loaded with DOX (DOX/PEG-MoS₂) (fig. S1F). After drug loading, the fingerprint anions belonging to MoS₂ nanosheets can still be clearly detected in LDI mass spectra of DOX/PEG-MoS₂ nanosheets (Fig. 1C). The characteristic peaks of DOX produced by the in-source decay (ISD) can also be detected by LDI MS at the same time (the peak assignment by HR MS and ISD fragment mechanism of DOX was shown in fig. S2). Here, the MoS₂
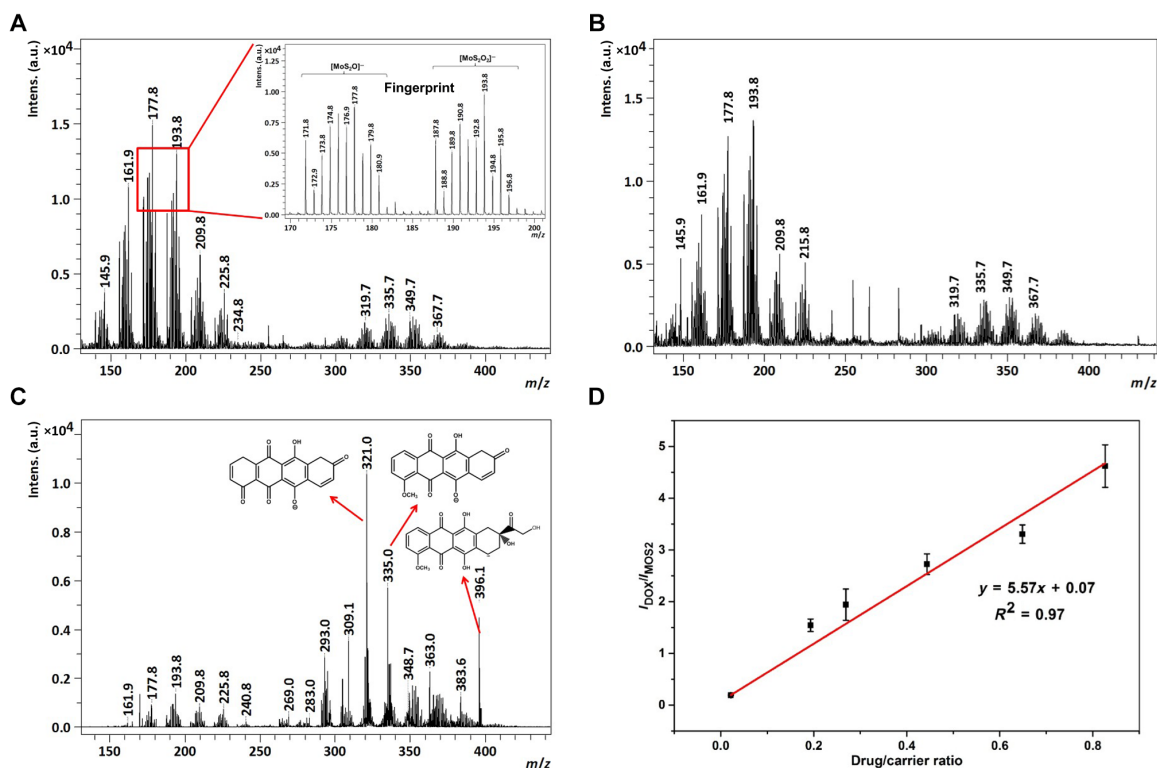

Fig. 1. MS characterization of MoS₂ nanosheets. (**A** to **C**) LDI mass spectra of (A) bare MoS₂ nanosheets, (B) PEG-MoS₂ nanosheets, and (C) DOX/PEG-MoS₂ nanosheets. (**D**) Calibration curve plotted average ion intensity ratio of DOX (m/z = 321.0) to MoS₂ nanosheets (m/z = 193.8) versus DOX loading ratio ([DOX]/[MoS₂ nanosheets]). The calibration curve was obtained by spiking DOX/PEG-MoS₂ nanosheets with a gradient drug/carrier ratio into a liver tissue homogenate. The fingerprint ion signals of mass spectra peaks are assigned as follows: m/z = 140.9 to 148.9, $[MoO_3]^-$; m/z = 155.9 to 163.9, $[MoO_4]^-$; m/z = 171.8 to 179.8, $[MoS_2O]^-$; m/z = 187.8 to 195.8, $[MoS_2O_2]^-$; m/z = 203.8 to 211.8, $[MoS_2O_3]^-$; and m/z = 219.8 to 227.8, $[MoS_2O_4]^-$. a.u., arbitrary units.

nanosheets may also serve as the matrix to assist the fragmentation and ionization of DOX to produce the final fragment product at $m/z = 321.0$, $m/z = 335.0$, and $m/z = 396.1$, which could easily be discriminated from the MoS₂ characteristic peaks around by HR TOF MS (fig. S2C), and these DOX characteristic peaks together discriminate the ion signal of DOX from other biological molecules in each tissue (figs. S2 and S11). We chose $m/z = 321.0$ (the highest-intensity mass peak) as the DOX signal in the following discussion. To confirm whether the ion at $m/z = 321.0$ is indeed from DOX, the MS/MS experiments were conducted. As shown in fig. S2, the evident MS/MS signals of $m/z = 321.0$ were observed from the tissues of DOX/PEG-MoS₂–injected mice (fig. S2G); particularly, these characteristic signals could match exactly to the MS/MS spectrum of the in vitro experiment (the DOX/PEG-MoS₂ nanosheets mixture was spotted directly on the MALDI target plate; fig. S2F). This result indicated that the MS/MS signals of $m/z = 321.0$ in tissues are derived from DOX. In addition, we also found that the ion intensity ratio of DOX over MoS₂ ($I_{m/z\ 321.0}/I_{m/z\ 193.8}$) was proportional to the loading ratio of DOX on the MoS₂ nanosheets. As shown in Fig. 1D, a good linear relationship was observed when plotting the ion intensity ratios of DOX over MoS₂ ($I_{m/z\ 321.0}/I_{m/z\ 193.8}$) versus different drug/carrier ratios in the homogenate of mouse liver tissue. Therefore, ion intensity ratio changes can reflect the drug/carrier ratio, which means that a decreased ratio will indicate the drug release from the nanocarriers. The intensity ratios of the DOX/PEG-MoS₂ with different loading ratios barely change in different tissue homogenates (fig. S3), although the absolute ion intensity of both nanocarriers and drugs may have differed slightly because of the influence of these different biological matrices. These results show the possibility of monitoring the drug release in tissues by easily measuring the MS ion intensity ratio of DOX over MoS₂.

Biodistribution of MoS₂ nanosheets in mice revealed by LDI MSI

The LDI MSI method was first attempted to investigate the circulation time and distribution behavior of bare and PEG-modified MoS₂ nanocarriers in normal mice (see the details in figs. S4 to S7 and the previous discussion in the Supplementary Materials). Predominant distributions were found in reticuloendothelial systems such as the lung, spleen, and liver with long retention time (more than 30 days for bare MoS₂ nanosheets). Studies have shown that the PEGylated MoS₂ nanosheets have faster excretion from the organs (19, 29), so we also compared the biodistribution of PEG-MoS₂ and bare MoS₂ in different tissues at 24 and 48 hours (fig. S6). The suborgan imaging results indicated faster clearance of PEG-MoS₂ from all of the studied tissues. The PEG-MoS₂ nanosheets could barely be observed in lung, kidney, heart, and brain tissues after a 48-hour circulation. Further investigation was carried out in two subcutaneous implanted tumor models: H22 and 4T1 tumor model mice (figs. S8 and S9 and the previous discussion). The LDI MSI images indicated much lower accumulation of MoS₂ nanosheets in tumor tissues when compared with the normal tissues. Direct comparison of the distribution of MoS₂ nanosheets in tumor-bearing tissue could minimize the influence brought by the growing
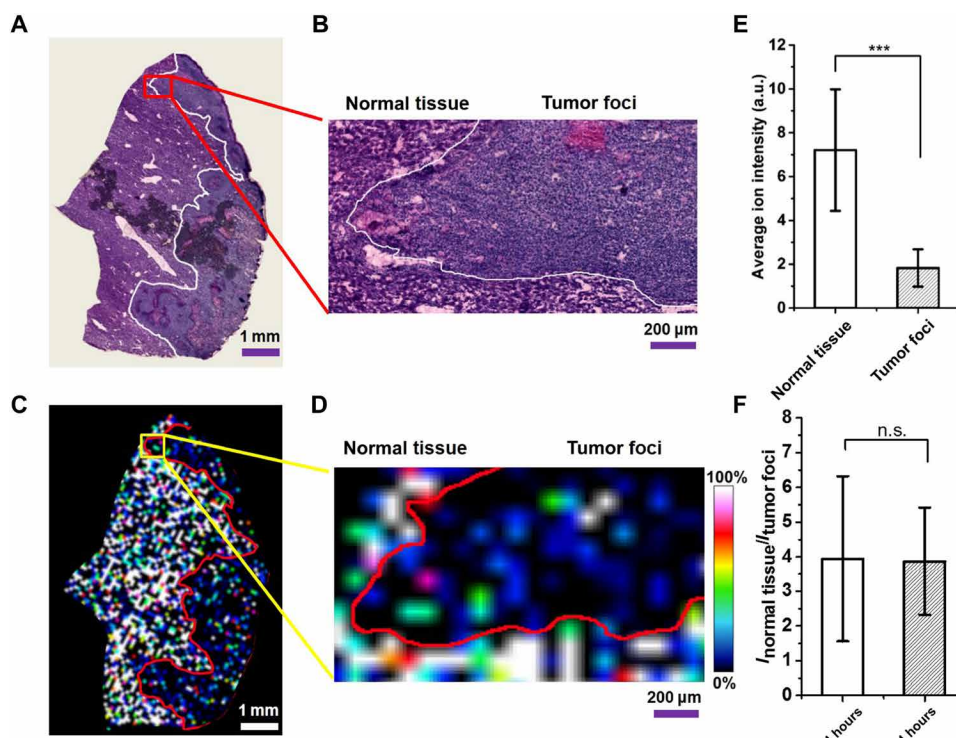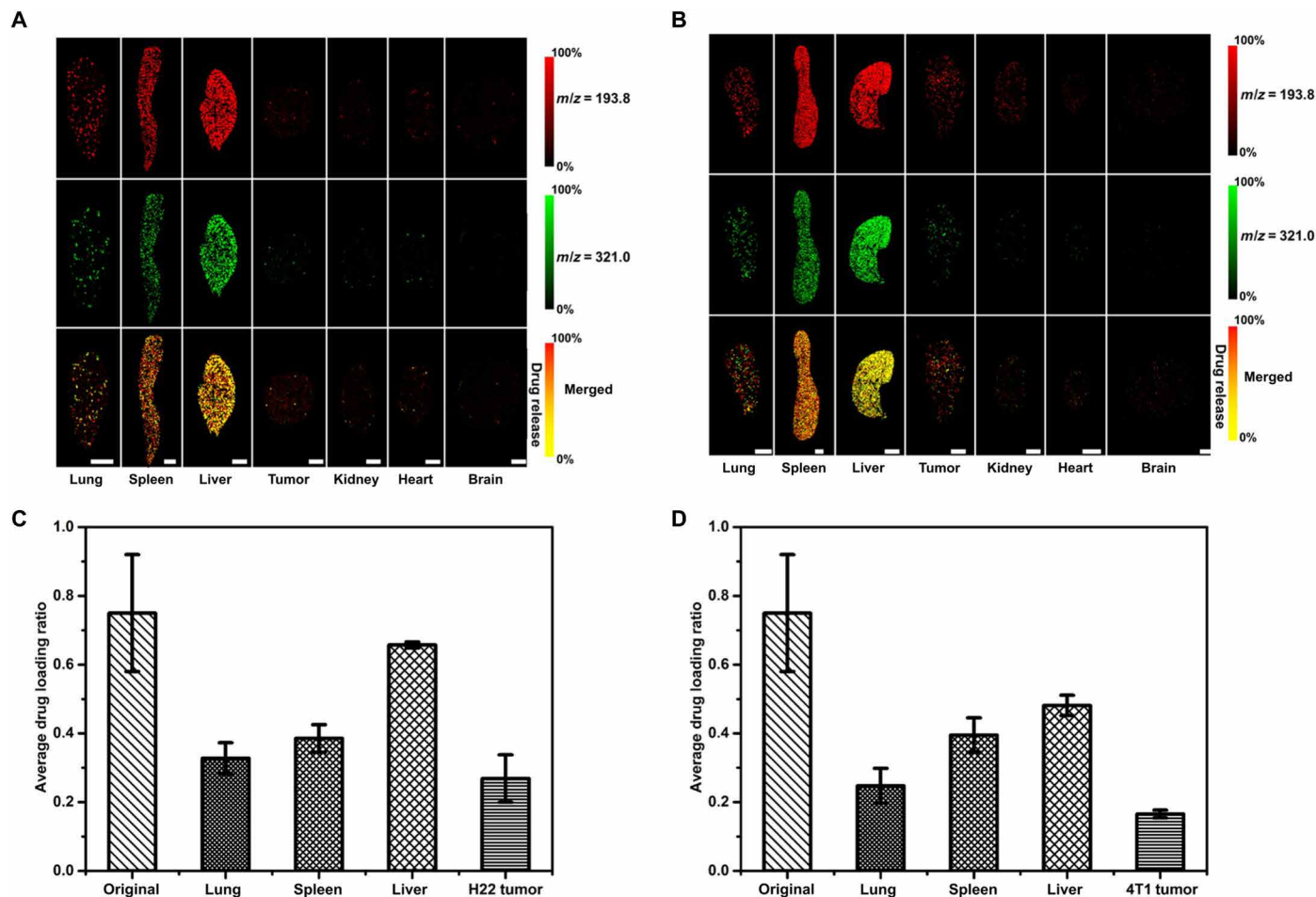

Fig. 2. Distribution of bare MoS₂ nanosheets in the liver of orthotopic H22 tumor model mice after 24-hour intravenous injection. (**A** and **B**) H&E-stained images of the (A) tumor-bearing liver tissue and (B) zoomed-in area of interest. (**C** and **D**) Corresponding LDI MSI images showing the distribution of bare MoS₂ nanosheets in (C) tumor-bearing liver tissue and (D) the corresponding zoomed-in area. (**E**) Average ion intensity of bare MoS₂ nanosheets in normal tissue and tumor foci. (**F**) Average ion intensity ratio of MoS₂ in normal tissue and tumor foci after 24- and 48-hour intravenous injection, respectively. Ten regions of interest (50 pixels each) were selected in both normal tissue and tumor foci. ***$P < 0.01$. n.s., no significant difference.

microenvironment difference of tumors and normal tissues (*30*). To achieve this aim, we carried out further LDI MSI experiments in H22 orthotopic tumor model mice. To differentiate the tumor foci and normal tissue, we performed hematoxylin and eosin (H&E) staining on the adjacent slice of the liver tissue that was sent to LDI MSI. Figure 2 shows the distribution of MoS_2 nanosheets in the tumor-bearing liver tissues. The LDI MSI images (Fig. 2, C and E) indicated the preferential accumulation of MoS_2 nanosheets in a normal region. The average ion intensity of MoS_2 nanosheets at m/z = 193.8 in the normal region is about 3.5-fold higher than that in tumor foci (Fig. 2E). Moreover, the intensity ratio of MoS_2 in the normal region over tumor foci has no notable difference after 24- and 48-hour circulations (Fig. 2F and fig. S10). These results provided the quantitative evidence that accumulation of MoS_2 nanosheets in tumor is much lower than in its normal counterpart, and this distribution ratio barely changes in a 2-day circulation. Collectively, the above studies demonstrated the ability of the proposed LDI MSI method for the suborgan mapping and semiquantitative comparison of the biodistribution of MoS_2 nanocarrier in normal and tumor-bearing tissues.

Evaluation of in vivo and in situ drug release of MoS₂ nanocarriers

One of the main concerns lying in the field of nanomedicine is to conveniently evaluate the in vivo and in situ drug release behavior (*4*). The proposed LDI MSI method enabling the simultaneous imaging of MoS_2 nanocarriers and payload drugs may address these issues. To validate this method, we first investigated the DOX/PEG-MoS_2 nanosheets in normal mice by LDI MSI after administration for 24 hours. As we expected, both the fingerprint ion signals of MoS_2 nanosheets (m/z = 198.3) and DOX (m/z = 321.0) can be detected in the studied organs (figs. S11 and S12). By merging these two ion intensities, the images show a high degree of overlapped distribution of MoS_2 nanosheets and DOX (fig. S11), which means that the drug-loaded nanocarriers successfully accumulated in these organs.

Further experiments were performed to investigate the drug release of the DOX/PEG-MoS_2 in tumor-bearing mice (Fig. 3). Figure 3 shows the distribution of DOX/PEG-MoS_2 in tissues of H22 and 4T1 subcutaneous implanted tumor models. Compared with other tissues, DOX/PEG-MoS_2 showed high accumulation in the spleen and liver, but the tumor tissue accumulation is much


Fig. 3. Biodistribution and drug release studies of DOX/PEG-MoS₂ revealed by LDI MSI. (**A** and **B**) Images of the biodistribution of DOX/PEG-MoS_2 nanosheets in tissues of (A) H22 and (B) 4T1 tumor model mice. (**C** and **D**) Average drug/carrier ratio in tissues of (C) H22 tumor and (D) 4T1 tumor models. The average drug/carrier ratios in each organ of (C) and (D) were obtained on the basis of the calibration curve in Fig.1D, by calculating the average ion intensity ratio of DOX (m/z = 321.0) over MoS_2 nanosheets (m/z = 193.8) in three randomly selected regions of corresponding organ (250 pixels each) in H22 and 4T1 tumor model mice, respectively. Scale bars, 5 mm. The statistical results shown in this figure were obtained from the mice that we show here, but we have tested three different mice in each group, and they all showed similar results.

lower. This distribution reflects the obstacles lying in the nanomedicine area for the limited tumor penetration and inefficient drug delivery drug to the tumor site (*31*). Meanwhile, the merged images show the different colors in different organs, indicating the different intensity ratio ($I_{m/z\ 193.8}/I_{m/z\ 321.0}$) in tissues. As mentioned before, the simultaneous detection of the MoS_2 nanosheets and the payload drug provides the opportunity to quantitatively compare the in vivo drug release through monitoring the change of ion intensity ratio ($I_{m/z\ 321.0}/I_{m/z\ 193.8}$), which is directly proportional to the drug/carrier ratio. The decreased ratio caused by the reduced ion intensity of DOX means that the drug is released from the nanocarriers. This result means that the drug release or dissociation could be in situ visualized by the LDI MSI method. As shown in Fig. 3 (C and D), the drug/carrier ratios in various tissues decreased after a 24-hour circulation when compared with the original value before the injection. The drug/carrier ratios even reduced over twofold in lung and tumor tissues. This reduction of the ratio indicated the release of the DOX from the nanocarriers in tissues. In addition, different tissues exhibited differential dissociation degrees. For example, the drug release in the liver is less than in other tissues in both of the two mice models. The lowest drug/carrier ratio was observed in both H22 and 4T1 tumor tissues, and about 63 and 76% of the drug were released or dissociated from carriers in these two tissues, respectively. This lowest drug/carrier ratio may be ascribed to high-

er drug dissociation extent due to a relatively lower pH value in the tumor microenvironment (*32*) and the slight degradation of MoS_2 nanosheets in tumor tissue. We have confirmed that the release of DOX from MoS_2 nanosheets is pH dependent (fig. S13), and the drug release rate and percentage increased along with the decrease of pH values. The released percentage of DOX in pH 5 (~30%) is about two times higher than that in pH 7.4 (~15%) after 48 hours. These results validated the feasibility of the proposed LDI MSI method to the in situ drug release study in tissues.

To further study the distribution and drug release and dissociation of DOX/PEG-MoS_2 in tumor-bearing tissues, we subjected liver tissue from the orthotopic H22 tumor model mice to LDI MSI analysis after the injection of these drug-loaded MoS_2 nanosheets. As shown in Fig. 4, the DOX/PEG-MoS_2 showed a similar inhomogeneous intratumoral distribution to the bare MoS_2 nanosheets. Further, relatively quantitative results show that the average ion intensity of DOX/PEG-MoS_2 in normal tissue is about four times higher than in its tumor counterpart after a 24-hour circulation (Fig. 4E), which is consistent with the previous observation for the lower accumulation in tumor tissues. In addition, the different drug dissociation degree in normal liver tissue and tumor foci was observed by the comparison of drug/carrier ratios in these two regions (Fig. 4F). The drug/carrier ratio is about twofold lower in tumor foci, which is similar to the observation from the above subcutaneous implanted tumor models.
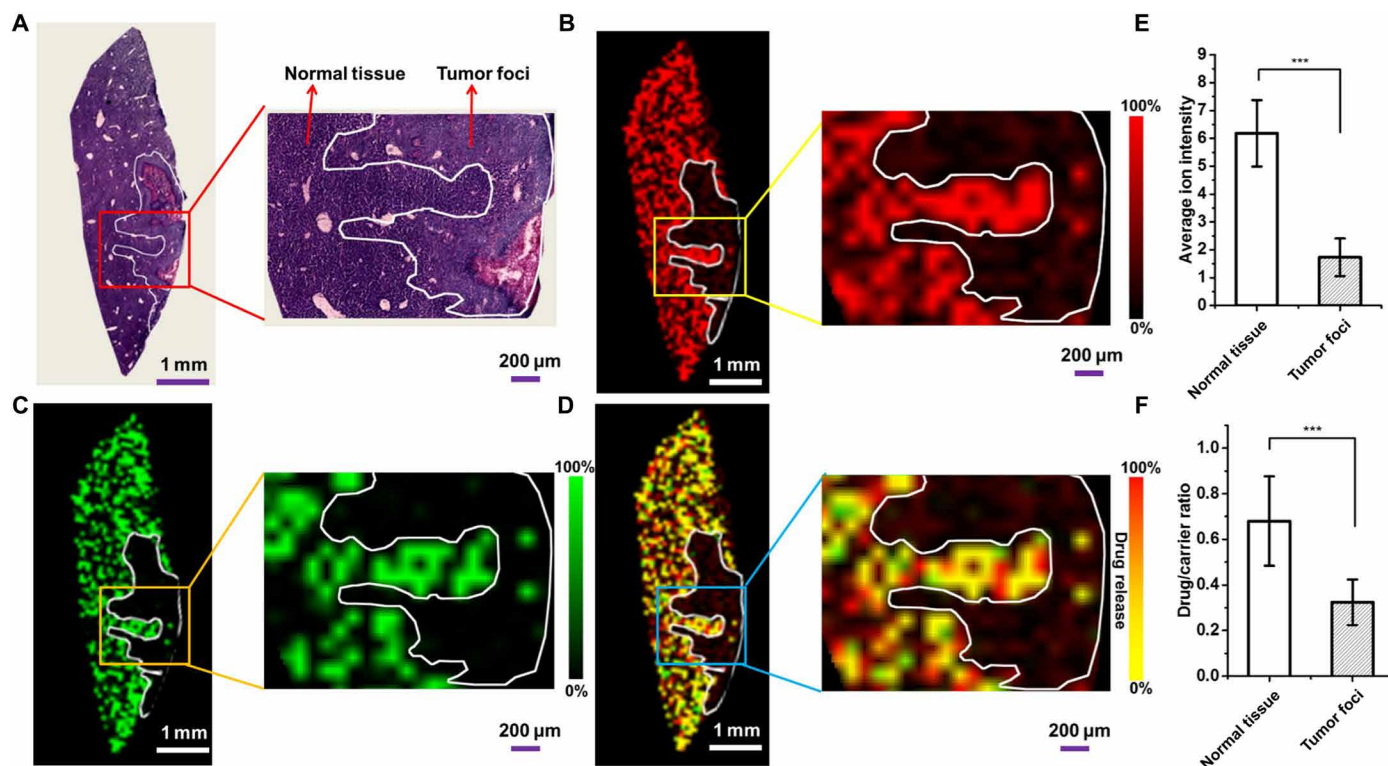
Fig. 4. Images of the distribution of MoS₂ nanosheets and their payload anticancer drug DOX in the liver tissue of orthotopic H22 tumor model mice after 24-hour intravenous injection. (**A**) H&E-stained image of the tumor-bearing liver tissue. The inset is the zoomed-in area of interest showing the normal tissue and tumor foci. (**B** and **C**) Corresponding LDI MSI images of DOX/PEG-MoS₂ nanosheets at (B) *m/z* = 193.8 and (C) *m/z* = 321.0 in tumor-bearing liver tissue. Insets show the detailed distribution information in normal tissue and tumor foci corresponding to the zoomed-in area. (**D**) Merged LDI MSI images of m/z = 193.8 and m/z = 321.0 in liver tumor-bearing liver tissues. (**E**) Average ion intensity of DOX/PEG-MoS₂ at *m/z* = 193.8 in normal tissue and tumor foci in (B). (**F**) Average drug/carrier ratio in normal tissue and tumor foci, which were obtained by calculating the average ion intensity ratio ($I_{m/z\ 321.0}/I_{m/z\ 193.8}$) in 10 randomly selected regions of normal liver tissue and tumor foci (50 pixels each), respectively. ***P < 0.01. The statistical results shown in this figure were obtained from the mice that we showed in this figure, but we have done three different mice in each group, and they all showed similar results.

As mentioned before, this proposed method could be applied to image other inorganic nanocarriers, e.g., drug-loaded carbon nanotubes, drug-loaded black phosphorus, and commonly used gold nanoparticles (figs. S14 to S16). All abovementioned three nanomaterials and their payload drugs can be simultaneously tracked and, therefore, can monitor the drug release or dissociation from these nanocarriers. The results show that our method is not restricted to one specific material but can also be extended to other nanocarrier–drug systems. Although the MALDI MSI was reported to simultaneously image the liposomal markers of liposomal carriers and the mimic cargo indocyanine green (33), our method shows advantages for the measuring of the real drug without an extra matrix, and the drug release could be semiquantitatively measured and read out from the imaging results.

Quantification of uptake of MoS₂ nanosheets in organs

The LDI MSI method could also quantify the uptake of MoS_2 nanosheets in tissues of mice bearing different times after injection (see details in the quantification method; fig. S17). The quantification results [percentage of injected dose (ID%)] are shown in Fig. 5, and MoS_2 nanosheets showed predominant accumulation in the lung within our studied time courses (Fig. 5B). The uptake of MoS_2 nanosheets in all three organs reached the maximum 24 hours after injection and then decreased with time prolonged, but there was still about 5 ID% remaining in the lung, spleen, and liver even after 30 days, demonstrating the long retention time of MoS_2 nanosheets

in tissues. However, the PEG modification may accelerate the clearance of MoS_2 nanosheets from tissues. It has been reported that PEG-MoS_2 could be excreted from the body almost completely within 30 days (29). We also compared our LDI MSI quantification with inductively coupled plasma MS (ICP-MS) to ensure the reliability of our method (Fig. 5C). The quantification of ICP-MS showed a higher Mo element amount in each organ than LDI MSI. Given that the ICP-MS measured the total Mo element in tissues, this slight difference may be ascribed to the existing Mo element in animals (control in Fig. 5C) or the Mo dissolved from MoS_2 nanosheets in biosystems (28, 34). This result also implies the advantage of the proposed LDI MSI method in the quantification of intact MoS_2 nanosheets. We further extended this method to the quantification of MoS_2 nanosheets in the lung, liver, and spleen and 4T1 tumor in tumor-bearing mice (Fig. 5D), and we observed the lower uptake of the nanocarriers in tumor compared with other organs. Thus, the proposed LDI MSI method combining the imaging and quantitative advantage provided a more comprehensive technique for the investigation of the biodistribution of nanocarriers in animals.

In summary, a novel label-free LDI MSI technique was developed and validated for the study of the in vivo and in situ drug release at the suborgan level. This strategy demonstrated a new paradigm for the analysis of drug release behavior by monitoring the MS intensities ratio of loaded drug and nanocarriers. With this method, the biodistribution of bare and DOX-loaded MoS_2 nanosheets was
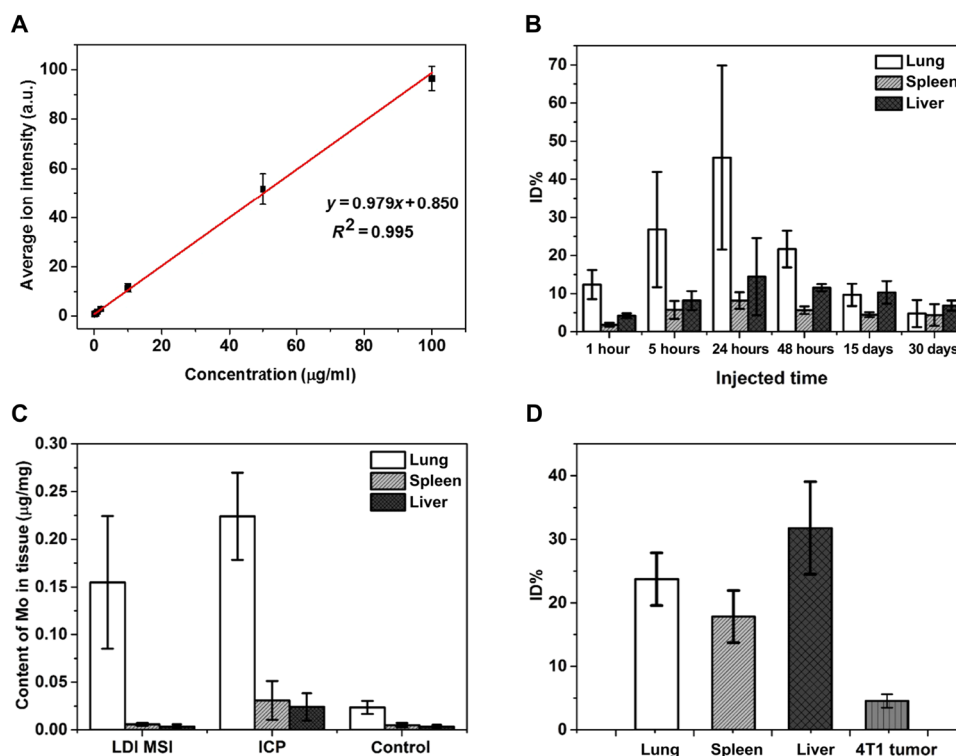
Fig. 5. Quantification of MoS₂ nanosheets in organs. (**A**) Calibration curve plotted average ion intensities of m/z = 193.8 against concentrations of MoS_2 nanosheets in spleen homogenate. (**B**) Quantification results of bare MoS_2 nanosheets in different organs varied with different time courses. (**C**) Comparative quantification of Mo element in different organs by LDI MS and ICP MS. The control group showed the content of Mo element in normal Kunming mice (three normal mice were tested) detected by ICP MS. (**D**) Quantification of MoS_2 nanosheets in the lung, spleen, and liver and 4T1 tumor of 4T1 tumor model mice bearing 24-hour intravenous injection of DOX/PEG-MoS_2.

visually compared in different organ tissues, and more importantly, the in situ release behavior of DOX among the tissues and inside tumor-bearing tissue was quantitatively investigated. It was observed that both the bare and drug-loaded MoS_2 nanocarriers were predominantly distributed in lung, spleen, and liver tissues, whereas the accumulation in the tumor is significantly lower than in normal tissues. The drug release study revealed the evident tissue-dependent releasing characteristics of DOX and provided the direct evidence that the drug release was promoted in tumor tissues. The long retention time up to 30 days of the bare MoS_2 nanocarriers was also observed in tissues. This strategy exhibited a unique advantage of both the imaging and quantitative analysis and may be extended to other nanocarrier-drug systems and thus can be used as a general approach to assist the design and evaluation of new nanotherapeutic systems.

MATERIALS AND METHODS
Materials and chemicals
MoS_2 powder was purchased from Sigma-Aldrich (USA). LA, *n*-butyllithium solution, and DOX hydrochloride were purchased from J&K Chemical Ltd. (Beijing, China). PEG polymers were purchased from Seebio Biotech Inc. (Shanghai, China). All high-performance liquid chromatography–grade solvents were purchased from Beihua Chemicals Inc. (China). Deionized water was purified using a Milli-Q Integral water purification system (Millipore, USA). Multiwalled carbon nanotubes (length, 5 to 20 nm) were purchased from Nanjing XFNANO Materials Tech Co. Ltd. (Nanjing, China). Black phosphorus powder was purchased from Sante Materials Tech Co. Ltd. (Taizhou, China).

Synthesis and characterization of single- and few-layered MoS_2 nanosheets
Morrison method (27) was used in this paper to synthesize single- and few-layered MoS_2 nanosheets. Briefly, 5 ml of 1.6 M *n*-butyllithium solution in hexane was added into 500 mg of MoS_2 powder under a nitrogen atmosphere and then stirred for 48 hours at room temperature to complete lithium intercalation. After that, the mixture was filtered to remove unreacted lithium, and the semidry mixture on the filter was washed with 100 ml of hexane to remove other organic residues. Then, the mixture was quickly immersed into 150 ml of deionized water and ultrasonicated for 1 hour to effectively achieve exfoliation. The exfoliated MoS_2 nanosheets were then centrifuged and washed with deionized water to remove LiOH precipitates and unexfoliated MoS_2. Last, the obtained MoS_2 nanosheet solution was dialyzed against deionized water using membranes [molecular weight cutoff (MWCO), 14 kDa] for 2 days and then stored at 4°C for future use. The synthesized single- and few-layered MoS_2 nanosheets were characterized by TEM [HRTEM, JEM-2011, JEOL (Japan)], UV-vis spectroscopy [TU1900, Purkinje General Instrument Co. Ltd. (Beijing, China)], and Fourier transform infrared spectroscopy [TENSOR-27, Bruker Optics (Germany)].

Modification of MoS_2 nanosheets with LA-PEG
Modification of MoS_2 nanosheets with LA-PEG was accomplished according to a previous report (19). Briefly, 100 mg of LA-PEG was mixed with 10 mg of bare MoS_2 nanosheets in 20 ml of deionized water; after sonication for 20 min, the mixed solution was stirred at room temperature for 24 hours to achieve the LA-PEG modification.

Then, excess LA-PEG was removed by ultracentrifugation with a Millipore centrifugal filter device (MWCO, 100 kDa).

Drug loading
DOX was loaded on the LA-PEG–modified MoS_2 nanosheets by mixing the PEG-MoS_2 nanosheets (0.2 mg/ml) with saturated DOX solution [in 10 mM PBS (phosphate-buffered saline) buffer (pH 8.0)] and stirring at room temperature for 24 hours. After loading, the excess free DOX was removed by centrifugal filtration and washed with PBS buffer several times. The amount of loading DOX was determined by measuring the characteristic peak intensity UV-vis adsorption spectra of PEG-MoS_2 nanosheets and DOX/PEG-MoS_2 nanosheets. The concentration of PEG-MoS_2 nanosheets was determined by adsorption at 808 nm, and the concentration of DOX was determined by adsorption at 490 nm after subtracting the contribution by PEG-MoS_2 nanosheets.

Animal care
Male Kunming mice (25 to 30 g) and female Balb/c mice were purchased from the Experimental Animal Center of the Academy of Military Medical Sciences. The animal experiments were performed according to the NIH Guide for the Care and Use of Laboratory Animals (National Institutes of Health Publication, No. 3040-2, revised 1999, Bethesda, MD) and were approved by the Animal Care and Use Committee of the Chinese Academy of Sciences.

Intravenous administration of bare MoS_2 nanosheets and drug loading MoS_2 nanosheets in mice
Bare MoS_2 nanosheets were injected into the normal and tumor-bearing mice through the tail vein with the dose of 5 mg/kg. The intravenous doses of MoS_2/PEG-DOX used for normal and tumor-bearing mice were 5 mg/kg for MoS_2 nanosheets and 3.5 mg/kg for DOX.

Tissue preparation
Male Kunming mice and female Balb/c mice injected with MoS_2 nanosheets or DOX/PEG-MoS_2 nanosheets were sacrificed by cervical dislocation after a specified time period, and organs studied in this paper were harvested within 10 min. Harvest organs were snap-frozen in liquid nitrogen and then stored in the fridge at −20°C. Before LDI MSI, the frozen tissues were cryosectioned at 10-μm-thick sections using a Leica CM1950 cryostat [Leica Biosystems (Nussloch, Germany)], and then, tissue sections were thaw-mounted onto the conductive side of an indium tin oxide (ITO)–coated glass slide [Bruker Daltonics (Bremen, Germany)]. For tissues that need H&E staining, tissues adjacent to the section for LDI MSI were mounted onto adhesion microscope slides. The ITO-coated glass slides with tissues were placed into a vacuum desiccator for about 30 min to completely dry the tissue.

Laser desorption/ionization mass spectrometry imaging
MSI was performed in negative reflection mode on an Ultraflextreme MALDI-TOF/TOF mass spectrometer [Bruker Daltonics (Billerica, MA)] equipped with a smartbeam II Nd:YAG 355-nm laser. Each mass spectrometer was acquired by adding 200 laser shots with the laser operating at 2000 Hz. Spatial resolution for tissue section imaging was set as 50 to 100 μm, the spatial resolution of tissue homogenate imaging for quantification was set as 200 μm. Before imaging, the laser power energy was adjusted to the optimal energy to acquire

the best fingerprint ion signal of MoS_2 nanosheets and drug. For quantification, the laser energy was kept constant for the whole process. The FlexImaging 4.0 software provided by Bruker Daltonics was used to profile the MSI results.

SUPPLEMENTARY MATERIALS

Supplementary material for this article is available at http://advances.sciencemag.org/cgi/content/full/4/10/eaat9039/DC1

Supplementary Materials and Methods

Fig. S1. Characterization of MoS_2 nanosheets.
Fig. S2. Identification of DOX fingerprint mass peak.
Fig. S3. Average ion intensity ratios of the DOX/PEG-MoS_2 with different loading ratios.
Fig. S4. Representative LDI MS spectra in mice tissues.
Fig. S5. LDI MSI images of tissues in normal mice.
Fig. S6. LDI MSI images of tissues injected with bare and LA-PEG–modified MoS_2 nanosheets (PEG-MoS_2) in normal mice.
Fig. S7. Suborgan distribution of MoS_2 nanosheets in normal mouse spleen.
Fig. S8. H&E-stained images of tissues from the tumor model mice.
Fig. S9. LDI MSI images of tissues in subcutaneous implanted tumor models.
Fig. S10. Distribution of bare MoS_2 nanosheets in the liver of orthotopic H22 tumor model mice after 48-hour intravenous injection.
Fig. S11. LDI MSI images of MoS_2 nanosheets and their payload DOX in tissues of normal mice.
Fig. S12. Representative LDI mass spectra of DOX/PEG-MoS_2–injected mouse tissue slices.
Fig. S13. Drug release from DOX/PEG-MoS_2 nanosheets at different pH values as a function of time.
Fig. S14. LDI MSI images of CNTs (carbon nanotubes) and their payload DOX in tissues.
Fig. S15. LDI MSI images of black phosphorus nanosheets and their payload DOX in tissues.
Fig. S16. LDI MSI images of gold nanoparticles and their payload DOX in tissues.
Fig. S17. Standard calibration curves for bare MoS_2 nanosheets in tissues.
References (35–40)

REFERENCES AND NOTES

1. M. E. Davis, Z. G. Chen, D. M. Shin, Nanoparticle therapeutics: An emerging treatment modality for cancer. *Nat. Rev. Drug Discov.* **7**, 771–782 (2008).
2. E. K.-H. Chow, D. Ho, Cancer nanomedicine: From drug delivery to imaging. *Sci. Transl. Med.* **5**, 216rv4 (2013).
3. N. Bertrand, J. Wu, X. Xu, N. Kamaly, O. C. Farokhzad, Cancer nanotechnology: The impact of passive and active targeting in the era of modern cancer biology. *Adv. Drug Deliv. Rev.* **66**, 2–25 (2014).
4. J. A. Hubbell, A. Chilkoti, Chemistry. Nanomaterials for drug delivery. *Science* **337**, 303–305 (2012).
5. T. M. Allen, P. R. Cullis, Drug delivery systems: Entering the mainstream. *Science* **303**, 1818–1822 (2004).
6. T. Sun, Y. S. Zhang, B. Pang, D. C. Hyun, M. Yang, Y. Xia, Engineered nanoparticles for drug delivery in cancer therapy. *Angew. Chem. Int. Ed.* **53**, 12320–12364 (2014).
7. Y. Dai, C. Xu, X. Sun, X. Chen, Nanoparticle design strategies for enhanced anticancer therapy by exploiting the tumour microenvironment. *Chem. Soc. Rev.* **46**, 3830–3852 (2017).
8. X. Bai, S. Wang, S. Xu, L. Wang, Luminescent nanocarriers for simultaneous drug or gene delivery and imaging tracking. *TrAC Trends Anal. Chem.* **73**, 54–63 (2015).
9. R. Wang, L. Zhou, W. Wang, X. Li, F. Zhang, In vivo gastrointestinal drug-release monitoring through second near-infrared window fluorescent bioimaging with orally delivered microcarriers. *Nat. Commun.* **8**, 14702 (2017).
10. J. Soltwisch, H. Kettling, S. Vens-Cappell, M. Wiegelmann, J. Muthing, K. Dreisewerd, Mass spectrometry imaging with laser-induced postionization. *Science* **348**, 211–215 (2015).
11. M. Kompauer, S. Heiles, B. Spengler, Atmospheric pressure MALDI mass spectrometry imaging of tissues and cells at 1.4-μm lateral resolution. *Nat. Methods* **14**, 90–96 (2017).
12. H. Liu, R. Chen, J. Wang, S. Chen, C. Xiong, J. Wang, J. Hou, Q. He, N. Zhang, Z. Nie, L. Mao, 1,5-Diaminonaphthalene hydrochloride assisted laser desorption/ionization mass spectrometry imaging of small molecules in tissues following focal cerebral ischemia. *Anal. Chem.* **86**, 10114–10121 (2014).
13. D. S. Cornett, M. L. Reyzer, P. Chaurand, R. M. Caprioli, MALDI imaging mass spectrometry: Molecular snapshots of biochemical systems. *Nat. Methods* **4**, 828–833 (2007).
14. F. J. Troendle, C. D. Reddick, R. A. Yost, Detection of pharmaceutical compounds in tissue by matrix-assisted laser desorption/ionization and laser desorption/chemical ionization tandem mass spectrometry with a quadrupole ion trap. *J. Am. Soc. Mass Spectrom.* **10**, 1315–1321 (1999).
15. S. Chen, C. Xiong, H. Liu, Q. Wan, J. Hou, Q. He, A. Badu-Tawiah, Z. Nie, Mass spectrometry imaging reveals the sub-organ distribution of carbon nanomaterials. *Nat. Nanotechnol.* **10**, 176–182 (2015).
16. J. Wei, J. M. Buriak, G. Siuzdak, Desorption-ionization mass spectrometry on porous silicon. *Nature* **399**, 243–246 (1999).
17. Z.-J. Zhu, Y.-C. Yeh, R. Tang, B. Yan, J. Tamayo, R. W. Vachet, V. M. Rotello, Stability of quantum dots in live cells. *Nat. Chem.* **3**, 963–968 (2011).
18. X. Zhang, Z. Lai, C. Tan, H. Zhang, Solution-processed two-dimensional MoS_2 nanosheets: Preparation, hybridization, and applications. *Angew. Chem. Int. Ed.* **55**, 8816–8838 (2016).
19. T. Liu, C. Wang, X. Gu, H. Gong, L. Cheng, X. Shi, L. Feng, B. Sun, Z. Liu, Drug delivery with PEGylated MoS_2 nano-sheets for combined photothermal and chemotherapy of cancer. *Adv. Mater.* **26**, 3433–3440 (2014).
20. W. Yin, L. Yan, J. Yu, G. Tian, L. Zhou, X. Zheng, X. Zhang, Y. Yong, J. Li, Z. Gu, High-throughput synthesis of single-layer MoS_2 nanosheets as a near-infrared photothermal-triggered drug delivery for effective cancer therapy. *ACS Nano* **8**, 6922–6933 (2014).
21. X. Li, J. Shan, W. Zhang, S. Su, L. Yuwen, L. Wang, Recent advances in synthesis and biomedical applications of two-dimensional transition metal dichalcogenide nanosheets. *Small* **13**, 1602660 (2017).
22. H. Chen, T. Liu, Z. Su, L. Shang, G. Wei, 2D transition metal dichalcogenide nanosheets for photo/thermo-based tumor imaging and therapy. *Nanoscale Horiz.* **3**, 74–89 (2018).
23. Z. Kou, X. Wang, R. Yuan, H. Chen, Q. Zhi, L. Gao, B. Wang, Z. Guo, X. Xue, W. Cao, L. Guo, A promising gene delivery system developed from PEGylated MoS_2 nanosheets for gene therapy. *Nanoscale Res. Lett.* **9**, 587 (2014).
24. J. Kim, H. Kim, W. J. Kim, Single-layered MoS_2-PEI-PEG nanocomposite-mediated gene delivery controlled by photo and redox stimuli. *Small* **12**, 1184–1192 (2016).
25. S. Wang, X. Li, Y. Chen, X. Cai, H. Yao, W. Gao, Y. Zheng, X. An, J. Shi, H. Chen, A facile one-pot synthesis of a two-dimensional MoS_2/Bi_2S_3 composite theranostic nanosystem for multi-modality tumor imaging and therapy. *Adv. Mater.* **27**, 2775–2782 (2015).
26. B. Pelaz, C. Alexiou, R. A. Alvarez-Puebla, F. Alves, A. M. Andrews, S. Ashraf, L. P. Balogh, L. Ballerini, A. Bestetti, C. Brendel, S. Bosi, M. Carril, W. C. W. Chan, C. Chen, X. Chen, X. Chen, Z. Cheng, D. Cui, J. Du, C. Dullin, A. Escudero, N. Feliu, M. Gao, M. George, Y. Gogotsi, A. Grunweller, Z. Gu, N. J. Halas, N. Hampp, R. K. Hartmann, M. C. Hersam, P. Hunziker, J. Jian, X. Jiang, P. Jungebluth, P. Kadhiresan, K. Kataoka, A. Khademhosseini, J. Kopecek, N. A. Kotov, H. F. Krug, D. S. Lee, C.-M. Lehr, K. W. Leong, X.-J. Liang, M. L. Lim, L. M. Liz-Marzan, X. Ma, P. Macchiarini, H. Meng, H. Möhwald, P. Mulvaney, A. E. Nel, S. Nie, P. Nordlander, T. Okano, J. Oliveira, T. H. Park, R. M. Penner, M. Prato, V. Puntes, V. M. Rotello, A. Samarakoon, R. E. Schaak, Y. Shen, S. Sjöqvist, A. G. Skirtach, M. G. Soliman, M. M. Stevens, H.-W. Sung, B. Z. Tang, R. Tietze, B. N. Udugama, J. S. VanEpps, T. Weil, P. S. Weiss, I. Willner, Y. Wu, L. Yang, Z. Yue, Q. Zhang, Q. Zhang, X.-E. Zhang, Y. Zhao, X. Zhou, W. J. Parak, Diverse applications of nanomedicine. *ACS Nano* **11**, 2313–2381 (2017).
27. P. Joensen, R. F. Frindt, S. R. Morrison, Single-layer MoS_2. *Mater. Res. Bull.* **21**, 457–461 (1986).
28. Z. Wang, A. von dem Bussche, Y. Qiu, T. M. Valentin, K. Gion, A. B. Kane, R. H. Hurt, Chemical dissolution pathways of MoS_2 nanosheets in biological and environmental media. *Environ. Sci. Technol.* **50**, 7208–7217 (2016).
29. J. Hao, G. Song, T. Liu, X. Yi, K. Yang, L. Cheng, Z. Liu, In vivo long-term biodistribution, excretion, and toxicology of PEGylated transition-metal dichalcogenides MS_2 (M = Mo, W, Ti) nanosheets. *Adv. Sci.* **4**, 1600160 (2017).
30. L. He, D.-A. Tian, P.-Y. Li, X.-X. He, Mouse models of liver cancer: Progress and recommendations. *Oncotarget* **6**, 23306–23322 (2015).
31. Y. Nakamura, A. Mochida, P. L. Choyke, H. Kobayashi, Nanodrug delivery: Is the enhanced permeability and retention effect sufficient for curing cancer? *Bioconjug. Chem.* **27**, 2225–2238 (2016).
32. M. Kanamala, W. R. Wilson, M. Yang, B. D. Palmer, Z. Wu, Mechanisms and biomaterials in pH-responsive tumour targeted drug delivery: A review. *Biomaterials* **85**, 152–167 (2016).
33. A. Fülöp, D. A. Sammour, K. Erich, J. von Gerichten, P. van Hoogevest, R. Sandhoff, C. Hopf, Molecular imaging of brain localization of liposomes in mice using MALDI mass spectrometry. *Sci. Rep.* **6**, 33791 (2016).
34. G. Schwarz, R. R. Mendel, M. W. Ribbe, Molybdenum cofactors, enzymes and pathways. *Nature* **460**, 839–847 (2009).
35. W. Tao, X. Zhu, X. Yu, X. Zeng, Q. Xiao, X. Zhang, X. Ji, X. Wang, J. Shi, H. Zhang, L. Mei, Black phosphorus nanosheets as a robust delivery platform for cancer theranostics. *Adv. Mater.* **29**, 1603276 (2017).
36. J. Fang, H. Nakamura, H. Maeda, The EPR effect: Unique features of tumor blood vessels for drug delivery, factors involved, and limitations and augmentation of the effect. *Adv. Drug Deliv. Rev.* **63**, 136–151 (2011).
37. H. Maeda, H. Nakamura, J. Fang, The EPR effect for macromolecular drug delivery to solid tumors: Improvement of tumor uptake, lowering of systemic toxicity, and distinct tumor imaging in vivo. *Adv. Drug Deliv. Rev.* **65**, 71–79 (2013).
38. K. Cho, X. Wang, S. Nie, Z. G. Chen, D. M. Shin, Therapeutic nanoparticles for drug delivery in cancer. *Clin. Cancer Res.* **14**, 1310–1316 (2008).
39. J. Wang, W. Mao, L. L. Lock, J. Tang, M. Sui, W. Sun, H. Cui, D. Xu, Y. Shen, The role of micelle size in tumor accumulation, penetration, and treatment. *ACS Nano* **9**, 7195–7206 (2015).

40. R. K. Jain, T. Stylianopoulos, Delivering nanomedicine to solid tumors. *Nat. Rev. Clin. Oncol.* **7**, 653–664 (2010).

Citation: J. Xue, H. Liu, S. Chen, C. Xiong, L. Zhan, J. Sun, Z. Nie, Mass spectrometry imaging of the in situ drug release from nanocarriers. *Sci. Adv.* **4**, eaat9039 (2018).